Quantum advantage in charging cavity and spin batteries by repeated interactions

Raffaele Salvia [1,2,*] Martí Perarnau-Llobet [2] Géraldine Haack [2] Nicolas Brunner,[2] and Stefan Nimmrichter [3,†]

[1]*Scuola Normale Superiore, I-56127 Pisa, Italy*
[2]*Département de Physique Appliquée, Université de Genève, 1211 Genève, Switzerland*
[3]*Naturwissenschaftlich-Technische Fakultät, Universität Siegen, Siegen 57068, Germany*

Recently, an unconditional advantage has been demonstrated for the process of charging of a quantum battery in a collisional model [Seah *et al.*, Phys. Rev. Lett. **127**, 100601 (2021)]. Motivated by the question of whether such an advantage could be observed experimentally, we consider a model where the battery is described by a quantum harmonic oscillator or a large spin, charged via repeated interactions with a stream of qubit units. For both setups, we show that a quantum protocol can significantly outperform the most general adaptive classical schemes, leading to 90 and 38% higher charging power for the cavity and large spin batteries, respectively. Toward an experimental realization, we also characterize the robustness of this quantum advantage to imperfections (noise and decoherence) considering implementations with state-of-the-art micromasers and hybrid superconducting devices.

I. INTRODUCTION

One central aim of the field of quantum thermodynamics is to improve and fuel thermodynamic processes via quantum resources [1–4]. Promising results include enhancements in cooling [5–12] as well as in the power [13–18], efficiency [19–24], and reliability [25–31] of quantum engines compared with their classical counterparts. However, it is often debated if the potential gains outweigh the cost of preparing the quantum resources and whether the same output can be simulated by classical means [32–35]. One approach to overcome these criticisms is to devise quantum protocols that overcome arbitrary classical strategies given some thermodynamically relevant figure of merit (and a finite set of available resources, like time or energy) in analogy with quantum advantages developed in quantum metrology [36] or quantum computation [37].

A well-known setup to investigate quantum advantages in thermodynamics consists of quantum batteries, i.e., small quantum systems that store and provide energy [38,39]. Following pioneering works [40–42], it has been rigorously proven that entangling operations enable faster battery charging given a collection of quantum batteries [43–45]. In such collective processes, the roles of dissipation [46–52], many-body interactions [44,53–63], energy fluctuations [64–71], and coherence [72–76] have also been investigated. In parallel, various types of quantum systems have been considered

quantum batteries, ranging from qubit ensembles [42,69,77–83] and ladder models [67,84–90] to oscillators and flywheels [50,91–94]. One of the prime candidates for experimental proofs of principle is the Dicke model battery [77–79,95–97], in which an ensemble of qubits is charged by a collectively coupled oscillator mode (see also related proposals in waveguide quantum electrodynamics (QED) setups [73,98]). Recent efforts in cavity and circuit QED have brought about the first results [99,100].

In a recent article, some of us investigated quantum advantages in battery charging which are not of collective nature [87]. We considered a collisional model where a stream of qubit units sequentially interacts with an energy ladder, which stores the energy, thus playing the role of the battery. In that model, we showed that quantum-coherent processes (where the qubits contain quantum coherence in the energy basis) can outperform arbitrary classical incoherent processes in terms of charging power. However, the interaction between the qubit units and the energy ladder considered in Ref. [87] was chosen such that the transition rates from one battery level to the next were uniform across the whole ladder. In this paper, we extend these promising results to realistic physical setups. For that, we replace the ideal energy ladder of Ref. [87] by two different physical models of quantum batteries: (i) a quantum harmonic oscillator and (ii) a large spin system. These two models can be realized with state-of-the-art experimental platforms, including (i) a micromaser (i.e., a cavity QED charged by an atomic ensemble [101]) and a circuit QED setup [102] and (ii) hybrid circuit QED-magnetic systems [103,104]. For both models, we show that a suitably chosen coherent charging protocol can outperform the best incoherent adaptive charging protocol in terms of power. For the micromaser cavity model, we argue that this advantage can be observed even in the presence of state-of-the-art experimental values of environmental damping or decoherence.

*raffaele.salvia@sns.it
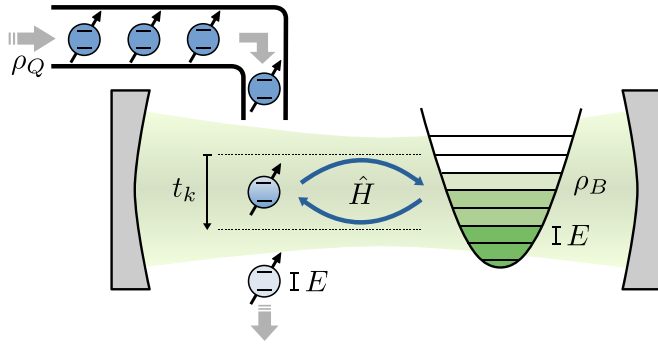†stefan.nimmrichter@uni-siegen.de

FIG. 1. Sketch of a micromaser as a quantum battery: Collisional charging of a harmonic oscillator battery (e.g., a cavity mode) by a sequence of identically prepared qubits. Each qubit carrying energy charge in its quantum state ρ_Q is allowed to exchange resonant excitations of energy E with the battery state ρ_B via the Hamiltonian $\hat{H}$. In adaptive protocols, the interaction times t_k can vary with the qubit number k.

The paper is organized as follows. In Sec. II, we describe the collisional model and relevant quantities. In Sec. III, we analyze the case of a harmonic oscillator battery. We derive an upper bound on the charging power for any adaptive incoherent protocol and demonstrate how to beat it with coherent protocols. We discuss possible realizations in cavity-QED and circuit-QED setups and show that the coherent quantum advantage can withstand weak damping due to photon loss. In Sec. IV, we present similar results for a large spin battery, which could be realized with hybrid circuits involving a superconducting qubit that would sequentially interact with a magnon [104]. Finally, we conclude in Sec. V.

II. FRAMEWORK

We first present some generic considerations for the sequential charging of the quantum battery by identical qubits, which serves as the basis for our treatment of oscillator and spin batteries. Let us consider the battery Hamiltonian $\hat{H}_B = E \sum_n n|n\rangle\langle n| = E\hat{N}$ describing a uniform, bounded or unbounded, energy ladder in steps of $E > 0$. Starting in the ground state of empty charge, $\rho_B(0) = |0\rangle\langle 0|$, the battery shall be charged by a sequence of resonant qubits with $\hat{H}_Q = E|e\rangle\langle e|$, as sketched in Fig. 1. Each qubit is prepared in a state:

$$\rho_Q = q|g\rangle\langle g| + (1-q)|e\rangle\langle e| + c\sqrt{q(1-q)}(e^{-i\alpha}|g\rangle$$
$$\times \langle e| + e^{i\alpha}|e\rangle\langle g|), \quad (1)$$

where $q \in [0, 1]$ is the ground-state population, $c \in [0, 1]$ is the amount of coherence in the state, and $\alpha \in [0, 2\pi]$ is a phase. Along this work, we make a distinction between quantum coherent protocols (where $c \neq 0$) and incoherent or classical protocols ($c = 0$).

In the kth step of the battery charging process, a qubit unit and the battery interact for a time t_k via the resonant exchange Hamiltonian:

$$\hat{H} = \Omega(\hat{A} \otimes |e\rangle\langle g| + \hat{A}^\dagger \otimes |g\rangle\langle e|), \quad (2)$$

at a fixed Rabi frequency Ω. Here, $\hat{A}$ represents a model-dependent ladder operator satisfying $\langle m|\hat{A}|n\rangle \propto \delta_{m,n-1}$. In our

previous work [87], we considered an ideal arithmetic energy ladder with $\hat{A} = \sum_{k=1} |k-1\rangle\langle k|$, which, although shown to be experimentally feasible [105,106], is not among the most readily available interactions in a laboratory, whereas here, we will focus on the following two physically relevant scenarios:

(i) a quantum harmonic oscillator, with $\hat{A}$ a bosonic annihilation operator, $\hat{A} = \hat{a} = \sum_{k=1} \sqrt{k} |k-1\rangle\langle k|$, and

(ii) large spin with $\hat{A} = \hat{J}_-$, the exact definition being introduced in Sec. IV.

Note that the total energy is preserved during the interaction process, $[\hat{H}, \hat{H}_B + \hat{H}_Q] = 0$, so that no additional work must be consumed in this process.

In the interaction picture with respect to $\hat{H}_B + \hat{H}_Q$, the state ρ_B of the battery evolves at the kth charging step as

$$\rho_B(k+1) = \text{tr}_Q\{\exp(-it_k\hat{H})\rho_B(k) \otimes \rho_Q \exp(it_k\hat{H})\}, \quad (3)$$

Such interaction processes are applied for a total available time τ, i.e.,

$$\tau = \sum_{k=1}^{K} t_k, \quad (4)$$

where K is the total number of qubits. We regard the charging time τ as the limiting resource, whereas K and $\{t_1, ..., t_K\}$ can be freely chosen with the only constraint of Eq. (4). In what follows, it will be convenient to introduce the dimensionless interaction times (swap angles):

$$\theta_k = \Omega t_k. \quad (5)$$

Our goal is to maximize the final average energy of the quantum battery, $\bar{E}(K) = \text{tr}\{\rho_B(K)\hat{H}_B\}$, under the time constraint τ. In other words, we wish to maximize the charging *power*:

$$\bar{\mathcal{P}} = \frac{\bar{E}(K)}{\tau}. \quad (6)$$

We will consider this optimization for both classical ($c = 0$) and quantum ($c \neq 0$) protocols. For convenience, we also introduce the transient charging power of the kth step:

$$\mathcal{P}(k) = \frac{\bar{E}(k) - \bar{E}(k-1)}{t_k}. \quad (7)$$

Although Eq. (6) is the central figure of merit of this work, we note that not all energy in $\rho_B(K)$ can be extracted as useful work. Some fraction of $\bar{E}(K)$ will be *passive* energy in the form of heat since the battery state has in general nonzero entropy. This motivates us to also compute the ergotropy $\mathcal{E}(K)$, which quantifies the amount of work that can be extracted from $\rho_B(K)$ in a cyclic Hamiltonian process [1,107]. Given a quantum state ρ with Hamiltonian $\hat{H}$, the ergotropy $\mathcal{E}$ is defined by $\mathcal{E} = \text{tr}\rho\hat{H} - \text{tr}\rho^{\text{passive}}\hat{H}$, where $\rho^{\text{passive}} = \sum_n r_n|n\rangle\langle n|$ with $[\rho^{\text{passive}}, \hat{H}] = 0$ and $\{r_n\}$ the eigenvalues of the initial state in descending order. Hence, the *useful* battery charge is always upper-bounded by the average energy, $\mathcal{E}_B \leqslant \bar{E}_B$, and equality only holds for pure battery states in our case.

Before moving forward, we also note that the evolution of the battery in Eq. (3) can be effectively described by a master equation model. While this approach is not strictly required to derive the main results presented in this paper, it is both
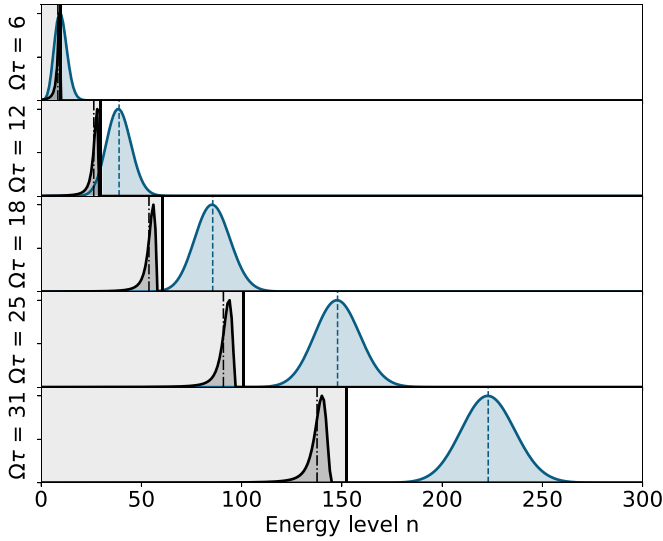
FIG. 2. Energy distribution of an oscillator battery at various charging times τ, comparing an exemplary coherent charging protocol (blue) to an adaptive incoherent protocol (black). The vertical lines mark the average energies. The former assumes qubits in a uniform superposition ($q = \frac{1}{2}$) and a constant interaction time $\theta = 0.01\pi$, whereas the latter operates with fully excited qubits ($q = 0$) and optimizes the charging time for maximum transient power in each step. The incoherent protocol beats deterministic charging via full swaps (dashed vertical line) but does not reach the incoherent power bound (gray shade boundary).

physically insightful and technically useful (e.g., for assessing the quantum-coherent evolution of the battery). We present it in detail in Appendix A for the interested reader.

III. HARMONIC OSCILLATOR BATTERY

We first consider the battery to be a quantum harmonic oscillator with Hamiltonian $\hat{H}_B = E\hat{a}^{\dagger}\hat{a}$ and interacting Hamiltonian:

$$\hat{H} = \Omega(\hat{a} \otimes |e\rangle\langle g| + \hat{a}^{\dagger} \otimes |g\rangle\langle e|). \quad (8)$$

For this micromaser model, Fig. 2 displays snapshots of the collisional battery charging. Indeed, it displays the battery energy distribution at increasing times during exemplary charging protocols. We compare coherent charging (blue) by weakly interacting qubits in the $|+\rangle$ state ($\theta = 0.01\pi$, $q = \frac{1}{2}$) to an adaptive protocol (black) with fully excited qubits ($q = 0$), in which we optimize the interaction time θ_k in each step for maximum transient power. This latter protocol outperforms a deterministic protocol of full excitation swap from each qubit (dashed vertical line), defined by $q = 0$ and $\theta_k = \pi/2 \ \forall k$. However, it cannot reach the coherent performance, as it must obey an incoherent bound on the charging power (gray shade boundary) that we will work out in the following. Finally, we also observe that the quantum randomlike behavior described in Ref. [87] (see Fig. 2 of [87]) is lost due to the different nature of the interaction.

A. Bound on the incoherent charging power

We first focus on incoherent charging strategies where $c = 0$ in Eq. (1). Let us expand $\hat{H}_B = E \sum_n n|n\rangle\langle n|$ and recall that, initially, the battery starts in the ground state, $\rho_B(0) = |0\rangle\langle 0|$. The state $\rho_B(k)$ remains energy-diagonal under the evolution in Eq. (3). The evolution of the populations $p(n, k) = \langle n| \rho_B(k) |n\rangle$ can be described by the rate equation:

$$p(n, k+1) = P_0(n, k)p(n, k) + P_-(n+1, k)p(n+1, k)$$
$$+ P_+(n-1, k)p(n-1, k), \quad (9)$$

where $P_-(n, k) = q \sin^2(\sqrt{n}\theta_k)$, $P_+(n, k) = (1 - q)\sin^2(\sqrt{n+1}\theta_k)$, and $P_0(n, k) = 1 - P_-(n, k) - P_+(n, k)$.

Consider the mean energy gain of the battery at the kth incoherent charge step:

$$\Delta\bar{E}(k) = \bar{E}(k) - \bar{E}(k-1)$$

$$= E \sum_{n=0}^{\infty} [P_+(n, k) - P_-(n, k)]p(n, k-1)$$

$$\leqslant E \sum_{n=0}^{\infty} \sin^2(\sqrt{n+1}\theta_k)p(n, k-1). \quad (10)$$

Naturally, this gain is optimal if we consider fully excited charge units ($q = 0$), as stated in the last line. Note that we assume that the swap angle θ_k can be adapted over the course of the sequence by changing the coupling time.

We now consider the transient charging power:

$$\frac{\mathcal{P}(k)}{E\Omega} = \frac{\Delta\bar{E}(k)}{E\theta_k} \leqslant \sum_{n=0}^{\infty} \frac{\sin^2(\sqrt{n+1}\theta_k)}{\theta_k}p(n, k-1). \quad (11)$$

It can be upper bounded by optimizing the level-dependent excitation rates over the swap angle (see also Ref. [93]):

$$\max_{\theta} \frac{\sin^2\left(\sqrt{n+1}\theta\right)}{\theta} = R_0\sqrt{n+1}, \quad (12)$$

with $R_0 \approx 0.725$ at $\theta \approx 0.742\,\pi/(2\sqrt{n+1})$. Inserting this result into Eq. (11) and making use of Jensen's inequality [108], we arrive at a nontight bound:

$$\frac{\mathcal{P}(k)}{E\Omega} \leqslant R_0 \sum_{n=0}^{\infty} \sqrt{n+1}\,p(n, k-1)$$

$$\leqslant R_0 \sqrt{\sum_{n=0}^{\infty}(n+1)p(n, k-1)}$$

$$= R_0 \sqrt{\frac{\bar{E}(k-1)}{E} + 1}. \quad (13)$$

Let us now define a continuous function $\bar{E}(\Omega\tau)$ of time that interpolates linearly between the values of the mean energy at successive charge steps. Following the derivation of Eq. (13), this function must satisfy

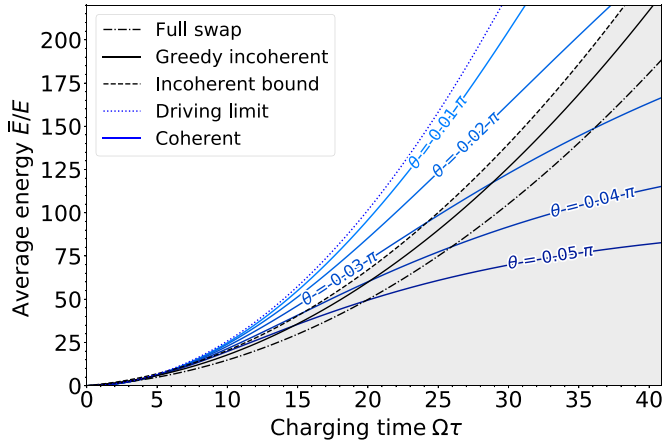$$\frac{d\bar{E}(\Omega\tau)}{d\tau} \leqslant \Omega E R_0 \sqrt{\frac{\bar{E}(\Omega\tau)}{E} + 1}, \quad (14)$$

FIG. 3. Collisional charging of a truncated harmonic oscillator battery with 250 levels, using coherent qubits in the $|+\rangle$ state ($q = 0.5$). Blue solid lines of darker shades show the mean battery energy $\bar{E}$ as a function of charging time $\Omega\tau = K\theta$ for increasing swap angles θ, while the blue dotted line represents the driving limit $\theta \to 0$. For comparison, the black dashed line marks the upper bound for adaptive incoherent charging strategies, closely approximated by a greedy protocol (black solid line) that optimizes the cumulatively averaged power at every charge step using excited qubits ($q = 0$). The dash-dotted line shows the deterministic full-swap protocol ($q = 0$, $\vartheta_k = \pi/2\sqrt{k}$) in which the battery remains in a pure charge state at all times.

which can be integrated by separation of variables. Given the initial condition $\bar{E}(0) = 0$, we arrive at the inequality:

$$\mathcal{E}(\Omega\tau) \leqslant \bar{E}(\Omega\tau) \leqslant E R_0 \Omega\tau \left(1 + \frac{R_0 \Omega\tau}{4}\right). \quad (15)$$

It gives an upper bound for the gain in mean energy (and thus ergotropy) after the charging time τ. Accordingly, it bounds the average charging power in Eq. (6) as

$$\bar{\mathcal{P}} \leqslant E\Omega R_0 \left(1 + \frac{R_0 \Omega\tau}{4}\right). \quad (16)$$

This bound is shown in Figs. 2–4, where it defines the gray region potentially accessible by classical charging protocols. We discuss the saturability of this upper bound by classical protocols in the next section.

B. Classical strategies

A natural candidate for an optimal classical strategy is a full-swap protocol: One decreases the interaction time in each charge step k according to $\vartheta_k = \pi/2\sqrt{k}$, such that the battery remains in a pure charge state, $p(n, k) = \delta_{nk}$, with the mean energy and ergotropy climbing up in steps of E. The corresponding transient power at the kth step is given by $\mathcal{P}(k) = \Omega \Delta \bar{E}(k)/\vartheta_k = 2\sqrt{k}\Omega E/\pi$. Assuming further that there is no waiting time between subsequent charge steps, the cumulative charging time is

$$\Omega\tau = \sum_{j=1}^{K} \vartheta_j = \frac{\pi}{2} \sum_{j=1}^{K} \frac{1}{\sqrt{j}} = \pi\sqrt{K} - \zeta_{1/2} + O\left\{\frac{1}{\sqrt{K}}\right\}, \quad (17)$$

with the Riemann zeta value $\zeta_{1/2} \approx 1.46$. Hence, the cumulatively averaged charging power becomes $\bar{\mathcal{P}} = \bar{E}(K)/\tau = KE/\tau \approx \mathcal{P}(K)/2$ for $K \gg 1$. Using Eq. (17), this can be expressed in terms of the total time as

$$\bar{\mathcal{P}} \approx \frac{E\Omega^2\tau}{\pi^2}. \quad (18)$$

For large τ, it reaches 0.77 of the upper bound in Eq. (16) (noting that both expressions grow linearly with τ).

By numerically optimizing over the interaction time, it is possible to find strategies that weakly outperform the full swap in terms of power. The example shown in Figs. 2 and 3 is the *greedy* incoherent protocol, i.e., the one that maximizes at each step the cumulative averaged power. We conclude that, while the bound in Eq. (16) is not tight, classical strategies can perform close to it. In what follows, we show that quantum strategies can outperform the classical bound.

C. Coherent charging

One can beat the incoherent bound in Eq. (15) in a nonadaptive protocol using pure coherent charge qubits and small swap angles θ. Specifically, for transient charging of an empty battery up to the Nth level, a coherent advantage can be achieved in the short time limit $\sqrt{N+1}\theta \ll 1$, where the charging process approximates a coherent driving term (see details in Appendix A). The best performance is obtained for equal superposition states with $q = \frac{1}{2}$ and $c = 1$ in Eq. (1), which yield the strongest driving amplitude.

In Fig. 3, we show the charging of an oscillator battery with such qubit states (at $\alpha = 0$) as a function of charging time $\Omega\tau = K\theta$, for various θ values and up to at most $N = 249$. The incoherent bound (dashed line) and the full-swap protocol (dash-dotted) are clearly beaten for $\theta \lesssim 1/\sqrt{250} \approx 0.02\pi$, whereas larger swap angles perform worse eventually.

Ideal performance is reached asymptotically in the short time limit $\theta \to 0$ (and $K \to \infty$), in which the battery state remains a pure displaced vacuum state at all times:

$$\rho_B(K) \xrightarrow[K\to\infty]{\theta\to0} \hat{D}\left(\frac{\Omega\tau}{2}\right)|0\rangle\langle 0|\hat{D}\left(-\frac{\Omega\tau}{2}\right), \quad (19)$$
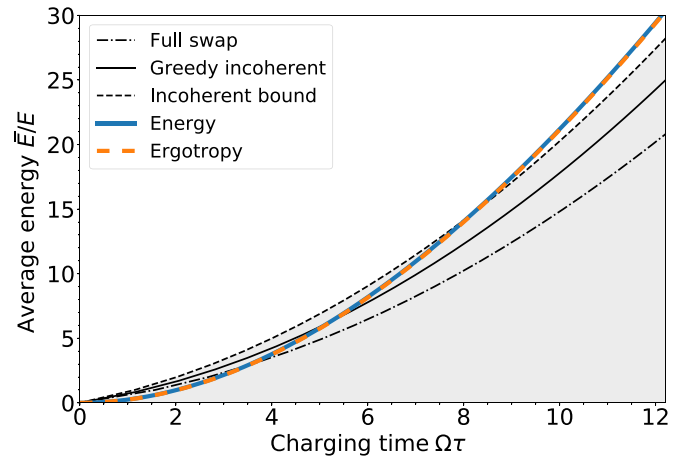

FIG. 4. Collisional charging of a truncated harmonic oscillator with 250 levels, using coherent qubits with $q = 0.5$ and a swap angle $\theta = 0.01\pi$, and with a damping of $\gamma = 10^{-3}$.

with $\hat{D}(\xi)$ the displacement operator. This follows from the small-θ expansion in Eq. (A13) of the coherent charging generator, which we perform in Appendix A for generic ladder batteries. The corresponding battery charge (dotted line) grows quadratically with time, $\mathcal{E}(\Omega\tau) = \bar{E}(\Omega\tau) = E(\Omega\tau)^2/4$, resulting in the average charging power:

$$\bar{\mathcal{P}} = \frac{E\,\Omega^2\tau}{4}. \qquad (20)$$

It outperforms the upper classical bound in Eq. (16) by a factor $R_0^{-2} \approx 1.90$—corresponding to a 90% quantum advantage. We stress that this is a theoretical limit in which each qubit unit transfers only infinitesimal amounts of energy (and thus wastes most of its useful energy) and the state of the battery remains pure. Nevertheless, in the next section, we show that the quantum advantage prevails in state-of-the-art experimental platforms with decoherence and a finite number of qubit units.

D. Photon loss and suitable experimental platforms

Several experimental platforms can correspond to a quantum battery modeled as a quantum harmonic oscillator, for instance, cold atoms and circuit QED setups. With these experimental platforms, it is important to assess the negative impact of photon loss on the coherent charging process, specifically the critical loss rate at which the quantum advantage disappears. To capture the effect of photon loss, we consider that subsequent charging steps are separated by a finite waiting time t_0 during which a fraction of the battery charge is lost. In realistic experimental implementations of this charging scheme, the waiting time typically will be much greater than the timescale of the collision (see the discussion below). Therefore, we only consider the photon loss that the cavity undergoes between consecutive collisions and neglect the dissipation that happens during each collision.

Employing the standard bosonic damping channel with rate κ, the battery state transforms in between subsequent charge steps according to the master equation $\partial_t \rho = \kappa\mathcal{D}[\hat{a}]\rho$, where $\mathcal{D}[\hat{M}]\rho = \hat{M}\rho\hat{M}^\dagger - \{\hat{M}^\dagger\hat{M}, \rho\}/2$. This results in the CPTP map [109]:

$$\Phi_0\rho_B = \exp(\kappa t_0 \mathcal{D}[\hat{a}])\rho_B = \sum_{n=0}^{\infty} \frac{[\exp(\kappa t_0) - 1]^n}{n!}\hat{K}_n\rho_B\hat{K}_n^\dagger,$$

$$\hat{K}_n = \hat{a}^n \exp\left(-\frac{\kappa t_0}{2}\hat{a}^\dagger\hat{a}\right). \qquad (21)$$

In the following, we employ the commonly used damping parameter $\gamma = 1 - \exp(-\kappa t_0)$, which approximates $\gamma \approx \kappa t_0$ when small.

Given this model of photon loss, we evaluate the cumulative charging power $\bar{\mathcal{P}}$ in Eq. (6) taking for τ the total time of the charging steps in which the qubit and battery interact (i.e., the preparation time of the qubit units is not accounted for in the charging power). The damping effect results in a correction of the incoherent charging limit in Eq. (15), see Appendix C for a derivation. Figure 5 plots the numerically evaluated point in time at which the coherent advantage first appears (i.e., the charging power exceeds the incoherent bound) as a function of θ for various γ values. It quickly
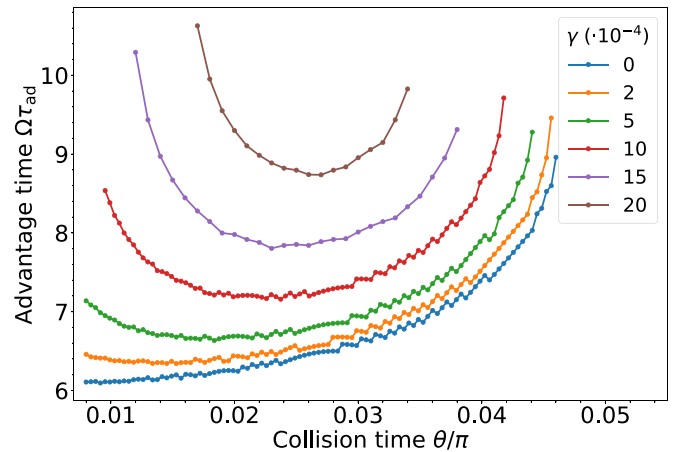

FIG. 5. Time τ_{ad} at which the energy of a cavity charged through collisions with constant interaction time θ and coherent qubits with $q = 0.5$ firstly overcomes the incoherent bound in Eq. (15) for different values of the intercollisional loss γ.

diverges with growing θ, and as γ reaches a critical value $\gtrsim 2 \times 10^{-3}$, above which the advantage is no longer there. For intermediate γ values, there is an optimal θ value for achieving the earliest coherent speedup in the protocol. We also observe that, as the best coherent charging protocols require small qubit-battery collision times θ, they are also vulnerable to small losses γ. For example, choosing $\theta = 0.01\pi$, a transient coherent advantage can be observed over a finite window of charging times for $\gamma = 10^{-3}$, as shown in Fig. 4.

The required loss value of the order of 10^{-3} can be achieved in state-of-the-art experiments. In the field of cold atoms, a setup like Ref. [101] could work. In this experiment, a high-quality microwave cavity would play the role of the battery, through which a sequence of individual atoms would be sent (the charging units). The state of individual atoms can be controlled via unitary operations, allowing for incoherent and coherent charging processes by tuning the parameter c as introduced in Eq. (1). Resonant interaction between the units and cavity could be implemented by choosing adequately the cavity mode. Moreover, projective energy measurements of the cavity and the charging atoms have been successfully implemented [101] and could be used to monitor the charging process. In the experimental setup of Ref. [101], a cavity with an inverse photon loss rate $1/\kappa \approx 65$ ms was made to collide with Rydberg atoms at intervals of $t_0 = 82\,\mu$s. This corresponds to a damping factor of $\gamma \approx 1.3 \times 10^{-3}$ between consecutive collisions, which is sufficiently low to support an observable quantum advantage in our model.

The Rabi frequency $\Omega = \Omega(t)$ varies with time, as it depends on the local intracavity field strength experienced by the atom. However, since we are assuming a resonant interaction, the Hamiltonian in Eq. (8) at different times commutes with itself, so that the coupling between the cavity and the atom will be given by an effective swap angle θ given by the time integral of the Rabi frequency over the atom trajectory, $\theta = \int dt\,\Omega(t)$. In Ref. [101], the velocity of the Rydberg atoms was selected to be $v = 250$ m/s, and the cavity had a waist of $w \simeq 6$ mm [110], which corresponds to an interaction time of the order of 10^{-5} s. The maximum Rabi frequency at the cen-

ter of the cavity was $\Omega_{\max} \simeq 50$ kHz [110], which allowed for large swap angles $\theta_{\max} \simeq \Omega_{\max} v/w > \pi/2$. The much smaller values of θ required for observing a charging advantage can be implemented by adjusting the impact parameter b of the atom trajectory with respect to the center of the cavity, which suppresses the local cavity field and thus the swap angle by a factor $\exp(-b^2/w^2)$ [111].

Superconducting platforms are also promising for demonstrating this quantum advantage. There, a microwave resonator would play the role of the battery, whereas a superconducting qubit repeatedly reinitialized in a coherent or incoherent state would play the role of the charging units. The resonant interaction between resonator and superconducting does correspond to flipflop-type interaction in the dispersive limit. As an example, we can cite a recent experiment [102], where a cavity with coherence time $100\,\mu s$ is coupled to a superconducting qubit. The cavity coherence time does include the cavity dissipation rate $\kappa/2\pi \sim 0.5$ MHz. Initialization and interaction times are estimated to be of the order of $10^{-1}\,\mu s$. This leads to a rate γ exceeding the value for which we predict a quantum advantage, but technological advances in this field are promising. The coherence time of $100\,\mu s$ would allow for simulating ~ 100 charging units.

IV. LARGE SPIN BATTERY

We will now discuss coherent and incoherent charging of a large spin battery. Following the previous section on suitable experimental platforms, in this case, we bring the attention of the reader to recent hybrid experiments manipulating magnons, either within a cavity-QED setup [103] or within circuit-QED circuits [104]. Magnons are quanta of collective spin excitations considering ordered magnetic phases. In Ref. [104], they manipulate a yttrium iron garnet (YIG) crystal magnetized by a uniform magnetic field. This leads to uniform magnetostatic mode (Kittel mode), which is coupled coherently with a superconducting transmon-type qubit. This constitutes the basic ingredients necessary for the charging protocol we propose, which we discuss in detail in what follows.

We assume a large spin battery, with half-integer or integer quantum number j and dimension $2j+1$. Its free Hamiltonian is given by the axial spin operator $\hat{H}_B = E\hat{J}_z = E\sum_{m=-j}^{j} m|j,m\rangle$, with eigenvectors $|j,m\rangle$. As before, the battery starts in the ground state $|j,-m\rangle$ and gets charged by a sequence of resonant qubits with $\hat{H}_Q = E|e\rangle\langle e|$, prepared in the state in Eq. (1). In each collision, the qubit and the battery interact for a time t_k through the energy-preserving exchange interaction Hamiltonian:

$$\hat{H} = \Omega(\hat{J}_- \otimes |e\rangle\langle g| + \hat{J}_+ \otimes |g\rangle\langle e|), \quad (22)$$

where the ladder angular momentum operators are defined by

$$\hat{J}_\pm |j,m\rangle = f_\pm(j,m)|j,m\pm 1\rangle,$$
$$f_\pm(j,m) = \sqrt{j(j+1)-m(m\pm 1)}. \quad (23)$$

We follow along the lines of Sec. III and first derive a nontight upper bound for adaptive incoherent charging protocols, we introduce the deterministic full-swap protocol, and finally, we show the coherent advantage.

A. Bound on the incoherent charging power

Starting from the ground state, $\rho_B(0) = |j,-m\rangle\langle j,-m|$, the state of the battery remains diagonal in the energy basis when charged by qubits without coherence. In full analogy with the rate equation in Eq. (9) for the oscillator case, and calling $\theta_k = \Omega t_k$, we can write the rates for jumping one step up and down the spin ladder as

$$P_-(m,k) = q\sin^2[f_-(m,k)\theta_k],$$
$$P_+(m,k) = (1-q)\sin^2[f_+(m,k)\theta_k],$$
$$P_0(m,k) = 1 - P_-(m,k) - P_+(m,k). \quad (24)$$

Consequently, the mean energy gain of the battery in the kth incoherent charge step reads as

$$\Delta\bar{E}(k) = E\sum_{m=-j}^{j}[P_+(m,k)-P_-(m,k)]p(m,k-1), \quad (25)$$

which is once again optimized by taking $q=0$ such that $P_-(m,k)=0$. Thus, in a completely analogous way as in Eq. (13), we can bound the transient charging rate of the spin battery by

$$\frac{\mathcal{P}(k)}{E\Omega} = \frac{\Delta\bar{E}(k)}{E\theta_k} \leqslant R_0 \sum_{m=-j}^{j} p(m,k-1)f_+(j,m)$$

$$\leqslant R_0 \sqrt{j(j+1) - \sum_{m=-j}^{j} p(m,k-1)m(m+1)}$$

$$\leqslant R_0\sqrt{j(j+1) - \mathrm{tr}\{(\hat{J}_z^2 - \hat{J}_z)\rho_B(k-1)\}}$$

$$\leqslant R_0\sqrt{j(j+1) - \langle J_z(k-1)\rangle^2 - \langle J_z(k-1)\rangle}, \quad (26)$$

with $\langle J_z(k)\rangle = \mathrm{tr}\{\hat{J}_z\rho_B(k)\} = \bar{E}(k)/E$. Interpolating this expectation value linearly between successive steps, we arrive at the differential inequality:

$$\frac{d\langle J_z(\Omega\tau)\rangle}{d\tau} \leqslant R_0\Omega\sqrt{j(j+1) - \langle J_z(\Omega\tau)\rangle(\langle J_z(\Omega\tau)\rangle + 1)}. \quad (27)$$

Given the initial condition $\langle J_z(0)\rangle = -j$, we can integrate Eq. (27) and obtain the inequality:

$$\arctan\left\{\frac{2\langle J_z(\Omega\tau)\rangle + 1}{2f_+[j, \langle J_z(\Omega\tau)\rangle]}\right\} - \arctan\frac{1-2j}{2} \leqslant R_0\Omega\tau. \quad (28)$$

The incoherent bound on the average charging power follows by setting both sides equal and solving for $\langle J_z(\Omega\tau)\rangle$, such that $\bar{\mathcal{P}} \leqslant E[\langle J_z(\Omega\tau)\rangle + j]/\tau$.

From Eq. (28), we can also estimate the time τ^* it takes to fully charge a large spin battery from $\langle J_z(0)\rangle = -j$ to $\langle J_z(\tau^*)\rangle = j$ with an incoherent protocol:

$$\tau^* \geqslant \frac{1}{R_0\Omega}\left(\arctan\frac{2j+1}{2} - \arctan\frac{1-2j}{2}\right)$$

$$\xrightarrow{j\to\infty} \frac{\arctan(\infty) - \arctan(-\infty)}{R_0\Omega}$$
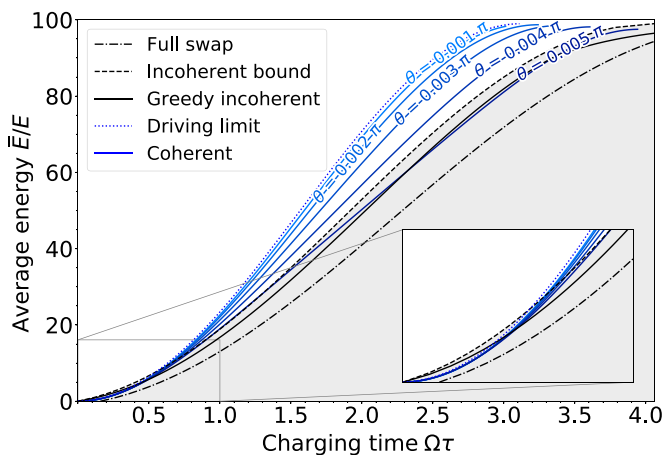
$$= \frac{\pi}{R_0\Omega}. \quad (29)$$

FIG. 6. Mean battery energy $\bar{E}$ as a function of charging time $\Omega\tau = k\theta$, for a spin-$\frac{99}{2}$ battery with 100 levels charged by a sequence of qubits. Blue solid lines of darker shades correspond to coherent qubits at $q = 0.5$ using increasing swap angles θ, and the blue dotted line corresponds to the driving limit $\theta \to 0$. The black dashed line marks the upper bound for adaptive incoherent charging strategies with excited qubits ($q = 0$), which is almost reached by a greedy protocol (black solid line) optimizing the cumulatively averaged power at every charge step. The dash-dotted line shows the less performant deterministic full-swap protocol. Inset: Zoom on the time interval where the coherent protocol for the charging process becomes better than the incoherent bound.

Hence, for a full charge at $j \gg 1$, the minimal time no longer depends on the number of battery levels due to the j scaling of the level-dependent coupling term in Eq. (23). Accordingly, the average power for a full incoherent charge of the battery does not exceed $\bar{\mathcal{P}}^* \leqslant 2E\,j\Omega R_0/\pi$.

B. Classical strategies

As in the oscillator case, we can consider a full-swap strategy in which we adapt the coupling times according to $\vartheta_k = \pi/2f_+(j,k)$, such that the battery is always in a pure charge state $|j, k - j\rangle$. The energy and ergotropy are equal and increase in steps of E. To completely charge the battery, $2j$ such swaps must be performed, which requires the total time:

$$\tau^* = \frac{1}{\Omega} \sum_{k=-j}^{j-1} \frac{\pi}{2f_+(j,k)} \xrightarrow{j \to \infty} \frac{\pi^2}{2\Omega}. \tag{30}$$

At $j \gg 1$, the overall charging power $\bar{\mathcal{P}} = 2E\,j/\tau^*$ is then $2/R_0\pi \simeq 0.88$ times lower than the incoherent upper bound deduced from Eq. (29).

A slightly better performance is obtained by the greedy incoherent protocol (shown in Fig. 6), which selects as the swap angle θ_k in each step the local maximum of the cumulative average charging power.

C. Coherent charging

The minimum full-charge time in Eq. (29) and the associated power bound hold for all incoherent protocols, but they can be overcome with coherent qubits. As for the oscillator

battery, the optimal performance is obtained with the choice $q = \frac{1}{2}$ and $c = 1$, regardless of the phase angle α. As an example, we compare coherent and incoherent charging protocols for a spin battery of dimension $d = 2j + 1 = 100$ in Fig. 6. We plot the average energy relative to the ground state $\bar{E}(K) + E\,j$ as a function of the charging time $\Omega\tau = \sum_{k=1}^{K} \theta_k$. The blue solid curves from light to dark correspond to non-adaptive coherent charging protocols ($q = \frac{1}{2}$, $c = 1$, and $\alpha = 0$) at growing values of the fixed swap angle $\theta_k = \theta$; they beat the incoherent bound (black dashed) when $\theta \lesssim 0.004\pi$. The optimized greedy incoherent protocol (black solid) gets close to the bound and clearly outperforms the full-swap protocol (dash-dotted).

The blue dotted line represents the asymptotic coherent driving limit $\theta \to 0$ in which the battery state remains pure and evolves according to

$$\rho_B(K) \xrightarrow[K \to \infty]{\theta \to 0} \hat{D}(\tau)|j, -j\rangle\langle j, -j|\hat{D}^\dagger(\tau). \tag{31}$$

Here, the unitary describes a coherent spin rotation by the angle $\Omega\tau$ about the x direction on the generalized Bloch sphere:

$$\hat{D}(\tau) = \exp\left[\frac{\Omega\tau}{2}(\hat{J}_+ + \hat{J}_-)\right]. \tag{32}$$

A complete charge of the battery corresponds to a π rotation, which requires the time $\tau^\star = \pi/\Omega$ and is therefore $R_0^{-1} \simeq 1.38$ times faster than the incoherent bound in Eq. (29), corresponding to a 38% quantum advantage.

V. CONCLUSIONS

Despite immense progress on our understanding of thermodynamics processes in the quantum regime [1–4], identifying quantum advantages in thermodynamics remains a challenging task. Quantum batteries offer a natural framework to explore this question and previous efforts focused on quantum advantages of a collective nature based on entanglement [38–45]. Building upon our previous work [87], here, we have shown that such quantum advantages can also appear at the level of a single battery: Given a collisional model of charging, we have proven that quantum coherent charging processes can outperform arbitrary classical charging strategies. More precisely, we have considered a set of qubit units that interact sequentially with a quantum battery, given by either a quantum harmonic oscillator (thus realizing a micromaser) or a large spin system. A quantum advantage arises in both setups, with 90 and 38% higher charging power through quantum resources for the micromaser and the spin batteries, respectively. We have characterized the robustness of the quantum advantage to decoherence and photon loss and discussed its feasibility in a cavity QED setup [101]. We also highlighted the possible implementation on a hybrid superconducting platform [103,104]. An experimental demonstration of these results is an exciting possibility that we hope can be achieved in the near future.

Note added. Upon finalizing this work, Ref. [112] appeared, which is also concerned with charging an oscillator battery with a sequence of coherent qubits in a micromaser setup. Complementary to our results, the authors focus on

the regime of ultrastrong cavity-qubit coupling and include counterrotating interaction terms in their model.

APPENDIX A: MASTER EQUATION MODEL FOR SEQUENTIAL BATTERY CHARGING

Here, we present a generic master equation model for the sequential charging of a ladder battery by identical qubits as described in the framework, Sec. II.

1. State change per charging step

Each charging step is represented by a unitary operation $\hat{U}$ acting on the combined Hilbert space of battery and qubit, which results in an effective quantum channel $\rho_B \mapsto \Phi\rho_B$, repeatedly applied to the reduced battery state. After k steps, we have $\rho_B(k) = \Phi^k\rho_B(0) = (1 + \mathcal{L})^k\rho_B(0)$. Given a Kraus representation of the channel, $\Phi\rho_B = \sum_i \hat{M}_i\rho_B\hat{M}_i^\dagger$ with $\sum_i \hat{M}_i^\dagger\hat{M}_i = \mathbb{1}$, we can express the incremental change of state $\mathcal{L}$ as a sum of Lindblad dissipators:

$$\mathcal{L}\rho_B := \Phi\rho_B - \rho_B = \sum_i \mathcal{D}[\hat{M}_i]\rho_B, \quad (A1)$$

using the abbreviation $\mathcal{D}[\hat{M}]\rho = \hat{M}\rho\hat{M}^\dagger - \{\hat{M}^\dagger\hat{M}, \rho\}/2$.

Here, one obtains a valid set of Kraus operators from the eigenbasis of the qubit state $\rho_Q = \sum_{n=0}^1 q_n|\psi_n\rangle\langle\psi_n|$ and an auxiliary orthonormal basis $\{|\chi_0\rangle, |\chi_1\rangle\}$:

$$\Phi\rho_B = \text{tr}\{\hat{U}\rho_B \otimes \rho_Q\hat{U}^\dagger\} = \sum_{m,n=0}^1 \hat{M}_{m,n}\rho_B\hat{M}_{m,n}^\dagger,$$

$$\hat{M}_{m,n} = \sqrt{q_n}\langle\chi_m|\hat{U}|\psi_n\rangle. \quad (A2)$$

One can easily check that $\sum_{m,n} \hat{M}_{m,n}^\dagger\hat{M}_{m,n} = \mathbb{1}$, given $q_0 + q_1 = 1$. This determines the master equations for incoherent and coherent charging, as expressed by the Lindblad generators $\mathcal{L}_{\text{inc}}$ and $\mathcal{L}_{\text{coh}}$.

For the incoherent case, the qubits are prepared in a mixed state $\rho_Q^{(\text{inc})}$ of a given ground-state probability q, i.e., $|\psi_0\rangle = |g\rangle$, $|\psi_1\rangle = |e\rangle$, and $q_0 = q$. Using the same auxiliary basis, we are left with

$$\mathcal{L}_{\text{inc}}\rho_B = q(\mathcal{D}[\langle g|\hat{U}|g\rangle] + \mathcal{D}[\langle e|\hat{U}|g\rangle])\rho_B$$

$$+ (1 - q)(\mathcal{D}[\langle g|\hat{U}|e\rangle] + \mathcal{D}[\langle e|\hat{U}|e\rangle])\rho_B. \quad (A3)$$

The amount of useful energy each qubit can at most transfer to the battery is specified by the ergotropy $\mathcal{E}_Q = \max\{0, 1 - 2q\}E \geqslant 0$. It is lower than the mean energy $(1 - q)E$ and finite only for population-inverted states ($q < \frac{1}{2}$).

For the coherent case of the same mean energy, the qubits are in a pure superposition state $\rho_Q^{(\text{coh})} = |\psi_0\rangle\langle\psi_0|$, with $|\psi_0\rangle = \sqrt{q}|g\rangle + \sqrt{1-q}e^{i\alpha}|e\rangle$ and $q_0 = 1$. The ergotropy

equals the mean energy $\mathcal{E}_Q = (1 - q)E$ and is nonzero also for $q > \frac{1}{2}$. To obtain the generator, we could construct an orthogonal complement to the qubit state $|\psi_1\rangle = \sqrt{1 - q}|g\rangle - \sqrt{q}e^{i\alpha}|e\rangle$, so that $\mathcal{L}_{\text{coh}}\rho_B = \mathcal{D}[\langle 0|\hat{U}|0\rangle]\rho_B + \mathcal{D}[\langle 1|\hat{U}|0\rangle]\rho_B$. However, it turns out to be more pertinent to use the energy states as the auxiliary basis and write

$$\mathcal{L}_{\text{coh}}\rho_B = \mathcal{D}[\langle g|\hat{U}|0\rangle]\rho_B + \mathcal{D}[\langle e|\hat{U}|0\rangle]\rho_B. \quad (A4)$$

This form ensures that, for the energy-preserving exchange interactions discussed next, the first dissipator can only contain excitations of the battery state, while the second dissipator can contain de-excitations only. Depending on the interaction model $\hat{U}$, one might be able to single out an explicit coherent driving term in the form of a Hamiltonian contribution to the master equation, with help of the identity:

$$\mathcal{D}[\hat{B} + \alpha\mathbb{1}]\rho = \mathcal{D}[\hat{B}]\rho + \left[\frac{\alpha^*\hat{B} - \alpha\hat{B}^\dagger}{2}, \rho\right]. \quad (A5)$$

Partially coherent qubit states of a given ground-state population q can always be written as a convex combination of the corresponding mixed and pure states $\rho_Q = c\rho_Q^{(\text{coh})} + (1 - c)c\rho_Q^{(\text{inc})}$, with $c \in [0, 1]$. This implies the same convex combination for the charging generator $\mathcal{L} = c\mathcal{L}_{\text{coh}} + (1 - c)\mathcal{L}_{\text{inc}}$. Ergotropy is then provided in the form of both coherence ($c > 0$) and population inversion ($q < \frac{1}{2}$) since $\mathcal{E}_Q = E[1 - 2q + \sqrt{(1 - 2q)^2 + 4c^2q(1 - q)}]/2$.

2. Energy-preserving resonant exchange

In our charging model, we demand that the battery charge be sourced exclusively by the charging qubits and that no additional work be consumed in the process. Hence, the interaction must be energy preserving, $[\hat{U}, \hat{H}_B + \hat{H}_Q] = 0$, and the associated quantum channel Φ a so-called thermal operation [113,114].

Specifically, we restrict our view to the resonant exchange of single excitations, as described by partial swap operations between the qubit and neighboring battery levels $\hat{U} = \exp(-i\hat{H}\theta)$ generated by a Hermitian coupling Hamiltonian of the form:

$$\hat{H} = \hat{A} \otimes |e\rangle\langle g| + \hat{A}^\dagger \otimes |g\rangle\langle e|, \quad \langle m|\hat{A}|n\rangle \propto \delta_{m,n-1}. \quad (A6)$$

Here, $\hat{A}$ represents a model-dependent ladder operator moving downward on the battery, while the parameter θ characterizes the level-dependent swap angle (including the coupling frequency Ω). For the studied cases of an oscillator and a spin battery in Secs. III and IV, we used $\hat{A} = \hat{a}$ and $\hat{A} = \hat{J}_-$, respectively. Note that the most general energy-preserving $\hat{H}$ could also contain phase-rotation terms of the form $\sum_n |n\rangle\langle n| \otimes (v_{n,e}|e\rangle\langle e| + v_{n,g}|g\rangle\langle g|)$. Such terms would complicate the charging dynamics and are not considered here.

The unitary charging operation can be expanded as

$$\hat{U} = e^{-i\hat{H}\theta} = \cos(|\hat{H}|\theta) - i\theta\text{sinc}(|\hat{H}|\theta)\hat{H}, \quad (A7)$$

introducing the absolute value operator:

$$|\hat{H}| := \sqrt{\hat{H}^2} = \sqrt{\hat{A}\hat{A}^\dagger \otimes |e\rangle\langle e| + \hat{A}^\dagger\hat{A} \otimes |g\rangle\langle g|}. \quad (A8)$$

It satisfies $[\hat{H}, |\hat{H}|] = 0$, and it is also diagonal in the product basis of battery and qubit energy states because $\hat{A}^\dagger\hat{A}$ and $\hat{A}\hat{A}^\dagger$

are diagonal in the basis of battery levels $|n\rangle$ by construction. However, $|\hat{H}|$ will not be full rank for (semi-)finite batteries with empty and fully charged states at $n = 0$ and $n = N$ (or $n \to \infty$) since $|0, g\rangle$ and $|N, e\rangle$ are not affected by $\hat{H}$.

From the matrix elements of the unitary, we can identify Lindblad operators $\hat{L}_-$ and $\hat{L}_+ = \hat{L}_-^\dagger$ associated to jumps down and up the battery ladder with level-dependent jump probabilities, as well as Lindblad operators $\hat{L}_{e,g} = \hat{L}_{e,g}^\dagger$ associated to dephasing between energy levels:

$$\hat{L}_g = \langle g|\hat{U}|g\rangle = \cos(\sqrt{\hat{A}^\dagger \hat{A}}\theta),$$

$$\hat{L}_e = \langle e|\hat{U}|e\rangle = (\sqrt{\hat{A}\hat{A}^\dagger}\theta),$$

$$\hat{L}_- = i\langle e|\hat{U}|g\rangle = \theta\,\mathrm{sinc}(\sqrt{\hat{A}\hat{A}^\dagger}\theta)\hat{A} = \theta\hat{A}\,\mathrm{sinc}(\sqrt{\hat{A}^\dagger\hat{A}}\theta),$$

$$\hat{L}_+ = i\langle g|\hat{U}|e\rangle = \hat{L}_-^\dagger. \qquad (A9)$$

In the third line, we make use of the fact that $(\hat{A}\hat{A}^\dagger)^k\hat{A} = \hat{A}(\hat{A}^\dagger\hat{A})^k$ for $k \in \mathbb{N}$ due to associativity. The generators for incoherent and coherent charging become

$$\mathcal{L}_{\mathrm{inc}}\rho_B = q(\mathcal{D}[\hat{L}_g] + \mathcal{D}[\hat{L}_-])\rho_B + (1-q)(\mathcal{D}[\hat{L}_e]$$
$$+ \mathcal{D}[\hat{L}_+])\rho_B, \qquad (A10)$$

$$\mathcal{L}_{\mathrm{coh}}\rho_B = \mathcal{D}[\sqrt{q}\hat{L}_- + i\sqrt{1-q}e^{i\alpha}\hat{L}_e]\rho_B + \mathcal{D}[\sqrt{1-q}\hat{L}_+$$
$$+ i\sqrt{q}e^{-i\alpha}\hat{L}_g]\rho_B. \qquad (A11)$$

For incoherent charging, the dephasing terms $\hat{L}_{e,g}$ can be ignored if there are no energy coherences in the battery state to begin with. The coherent process, on the other hand, will build up such coherences.

For small θ, we can expand the generators to second order in θ. By virtue of the identity in Eq. (A5), we arrive at

$$\mathcal{L}_{\mathrm{inc}}\rho_B \approx q\theta^2\mathcal{D}[\hat{A}]\rho_B + (1-q)\theta^2\mathcal{D}[\hat{A}^\dagger]\rho_B, \qquad (A12)$$

$$\mathcal{L}_{\mathrm{coh}}\rho_B \approx \mathcal{L}_{\mathrm{inc}}\rho_B - i\sqrt{q(1-q)}\theta[e^{-i\alpha}\hat{A} + e^{i\alpha}\hat{A}^\dagger, \rho_B]. \qquad (A13)$$

That is to say, in the limit of short or weak interactions, the incoherent charging process is always of second order in θ, whereas the coherent process adds an effective driving Hamiltonian $\hat{V} = \sqrt{q(1-q)}\theta e^{-i\alpha}\hat{A} + \mathrm{H.c.}$ The driving term is of first order in θ, and so it dominates whenever $q \neq 0, 1$. It preserves the purity of the battery state and is responsible for the coherent advantages we have discussed for oscillator and spin batteries.

In Appendix B, we derive explicit Lindblad operators for a uniform ladder battery and recover the random-walk charging process studied in Ref. [87]. There, we can make use of Eq. (A5) to single out a Hamiltonian driving term for the coherent case.

APPENDIX B: RANDOM-WALK BATTERY

Let us use our generic results and check consistency with the random-walk battery we have studied before in Ref. [87]. The uniform ladder operator is $\hat{A} = \sum_{n=1}^N |n-1\rangle\langle n|$, and we can quickly convince ourselves that

$$\hat{A}^\dagger\hat{A} = \mathbb{1} - |0\rangle\langle 0| = \sqrt{\hat{A}^\dagger\hat{A}}, \quad \hat{A}\hat{A}^\dagger = \mathbb{1} - |N\rangle\langle N| = \sqrt{\hat{A}\hat{A}^\dagger}. \qquad (B1)$$

These projectors imply that $f(\hat{A}\hat{A}^\dagger)\hat{A} = f(\mathbb{1})\hat{A}$ and $f(\hat{A}^\dagger\hat{A})\hat{A}^\dagger = f(\mathbb{1})\hat{A}^\dagger$. Hence, we get for the incoherent model:

$$\mathcal{L}_{\mathrm{inc}}\rho_B = q\sin^2\theta\mathcal{D}[\hat{A}]\rho_B + (1-q)\sin^2\theta\mathcal{D}[\hat{A}^\dagger]\rho_B + q\mathcal{D}[|0\rangle\langle 0| + (\mathbb{1} - |0\rangle\langle 0|)\cos\theta]\rho_B + (1-q)\mathcal{D}[|N\rangle\langle N|$$
$$+ (\mathbb{1} - |N\rangle\langle N|)\cos\theta]\rho_B = \sin^2\theta(q\mathcal{D}[\hat{A}] + (1-q)\mathcal{D}[\hat{A}^\dagger])\rho_B + (1-\cos\theta)^2\{q\mathcal{D}[|0\rangle\langle 0|] + (1-q)\mathcal{D}[|N\rangle\langle N|]\}\rho_B, \qquad (B2)$$

where, for the last line, we made use of Eq. (A5). The result is exactly what we got in Ref. [87]. The dephasing only affects the two boundary levels directly.

For the coherent model, we similarly get

$$\mathcal{L}_{\mathrm{coh}}\rho_B = \mathcal{D}\{\sqrt{q}\sin\theta\hat{A} + i\sqrt{1-q}e^{i\alpha}[\cos\theta\mathbb{1} + (1-\cos\theta)|0\rangle\langle 0|]\}\rho_B + \mathcal{D}\{\sqrt{1-q}\sin\theta\hat{A}^\dagger + ie^{-i\alpha}\sqrt{q}[\cos\theta\mathbb{1}$$
$$+ (1-\cos\theta)|N\rangle\langle N|]\}\rho_B = -i\sqrt{q(1-q)}\sin\theta\cos\theta[e^{-i\alpha}\hat{A} + e^{i\alpha}\hat{A}^\dagger, \rho_B] + \mathcal{D}[\sqrt{q}\sin\theta\hat{A}$$
$$+ i\sqrt{1-q}e^{i\alpha}(1-\cos\theta)|0\rangle\langle 0|]\rho_B + \mathcal{D}[\sqrt{1-q}\sin\theta\hat{A}^\dagger + ie^{-i\alpha}\sqrt{q}(1-\cos\theta)|N\rangle\langle N|]\rho_B. \qquad (B3)$$

Using again Eq. (A5) for the identity term inside the dissipators has lead us to our old result. However, we see that the appearance of an explicit driving Hamiltonian is due to the simple projectors in Eq. (B1), which cannot be expected for other models.

APPENDIX C: INCOHERENT CHARGING BOUND WITH DISSIPATION

Here, we derive an upper bound for the incoherent charging of an oscillator battery in the presence of damping. Our model

in Sec. III D assumes that the charging events are short and separated by a waiting time τ_0 during which the oscillator is subject to a (quantum-limited) attenuation channel in Eq. (21) with a damping constant γ.

We can restrict our view to excited qubits ($q = 0$) so that, in the charge step (ch), the battery either gains one charge unit E with probability $P_+(n) = \sin^2(\sqrt{n+1}\theta)$ or remains at its current level n with $P_0(n) = 1 - P_+(n)$. During the damping period that follows, the battery can only lose charge. Starting from the nth level, the energy loss due to damping is $\Delta E^{(\mathrm{da})}(n) = E\mathrm{tr}[\hat{a}^\dagger\hat{a}\Phi_0(|n\rangle\langle n|)] - En = -\gamma En$. Hence, like

Eq. (10), the combined mean energy change over the kth charging step with swap angle θ_k and the subsequent damping can be written as

$$\Delta \bar{E}(k) = E \sum_{n=0}^{\infty} p(n, k-1)\{P_+(n, k)[1 - \gamma(n+1)] - P_0(n, k)\gamma n\} = E \sum_{n=0}^{\infty} p(n, k-1)[(1-\gamma)\sin^2(\sqrt{n+1}\theta_k) - \gamma n]. \quad \text{(C1)}$$

In full analogy to Sec. III, we can now construct an upper bound on the transient charging power $\mathcal{P}(k) = \Omega \Delta \bar{E}(k)/\theta_k$ by maximizing and upper bounding each n summand individually:

$$\max_{\theta \in [0, \frac{\pi}{2}]} \frac{(1-\gamma)\sin^2(\sqrt{n+1}\theta) - \gamma n}{\theta} \leqslant (1-\gamma) \max_{\theta \in [0, \frac{\pi}{2}]} \frac{\sin^2(\sqrt{n+1}\theta)}{\theta} - \gamma \min_{\theta \in [0, \frac{\pi}{2}]} \frac{n}{\theta} = (1-\gamma)\sqrt{n+1}R_0 - \frac{2\gamma n}{\pi}. \quad \text{(C2)}$$

Note that, for the sake of clarity, we are only counting the charging time and omitting the damping time t_0 here. Otherwise, the overall charging time would be offset by Kt_0. Then Eq. (13) has to be modified to

$$\frac{\Delta \bar{E}(k)}{E\theta_k} \leqslant R_0(1-\gamma)\sqrt{\frac{\bar{E}(k-1)}{E} + 1} - \frac{2}{\pi}\gamma \bar{E}(k-1), \quad \text{(C3)}$$

and therefore (assuming a growing $\bar{E}$),

$$\frac{d\bar{E}(\Omega\tau)}{d\tau} \leqslant \Omega E R_0(1-\gamma)\sqrt{\frac{\bar{E}(\Omega\tau)}{E} + 1} - \frac{2\Omega}{\pi}\gamma \langle E(\Omega\tau)\rangle. \quad \text{(C4)}$$

The solution of Eq. (C4) gives a bound for the incoherent charging in the presence of dissipation; it does not differ appreciably from Eq. (15) in the considered weak-damping regime $\gamma \ll 1$.

---

[1] J. Goold, M. Huber, A. Riera, L. del Rio, and P. Skrzypczyk, The role of quantum information in thermodynamics—A topical review, J. Phys. A: Math. Theor. **49**, 143001 (2016).

[2] S. Vinjanampathy and J. Anders, Quantum thermodynamics, Contemp. Phys. **57**, 545 (2016).

[3] M. T. Mitchison, Quantum thermal absorption machines: Refrigerators, engines and clocks, Contemp. Phys. **60**, 164 (2019).

[4] N. M. Myers, O. Abah, and S. Deffner, Quantum thermodynamic devices: From theoretical proposals to experimental reality, AVS Quantum Sci. **4**, 027101 (2022).

[5] N. Brunner, M. Huber, N. Linden, S. Popescu, R. Silva, and P. Skrzypczyk, Entanglement enhances cooling in microscopic quantum refrigerators, Phys. Rev. E **89**, 032115 (2014).

[6] M. T. Mitchison, M. P. Woods, J. Prior, and M. Huber, Coherence-assisted single-shot cooling by quantum absorption refrigerators, New J. Phys. **17**, 115013 (2015).

[7] J. B. Brask and N. Brunner, Small quantum absorption refrigerator in the transient regime: Time scales, enhanced cooling, and entanglement, Phys. Rev. E **92**, 062101 (2015).

[8] P. P. Hofer, M. Perarnau-Llobet, J. B. Brask, R. Silva, M. Huber, and N. Brunner, Autonomous quantum refrigerator in a circuit QED architecture based on a Josephson junction, Phys. Rev. B **94**, 235420 (2016).

[9] M. T. Mitchison and P. P. Potts, Physical implementations of quantum absorption refrigerators, in *Thermodynamics in the Quantum Regime. Fundamental Theories of Physics*, edited by F. Binder, L. Correa, C. Gogolin, J. Anders, and G. Adesso (Springer, Cham, 2018), Vol. 195, pp. 149–174.

[10] V. Holubec and T. Novotný, Effects of noise-induced coherence on the performance of quantum absorption refrigerators, J. Low Temp. Phys. **192**, 147 (2018).

[11] K. E. Dorfman, D. Xu, and J. Cao, Efficiency at maximum power of a laser quantum heat engine enhanced by noise-induced coherence, Phys. Rev. E **97**, 042120 (2018).

[12] G. Maslennikov, S. Ding, R. Hablützel, J. Gan, A. Roulet, S. Nimmrichter, J. Dai, V. Scarani, and D. Matsukevich, Quantum absorption refrigerator with trapped ions, Nat. Commun. **10**, 202 (2019).

[13] U. Harbola, S. Rahav, and S. Mukamel, Quantum heat engines: A thermodynamic analysis of power and efficiency, Europhys. Lett. **99**, 50005 (2012).

[14] R. Uzdin, A. Levy, and R. Kosloff, Equivalence of Quantum Heat Machines, and Quantum-Thermodynamic Signatures, Phys. Rev. X **5**, 031044 (2015).

[15] G. Manzano, F. Galve, R. Zambrini, and J. M. R. Parrondo, Entropy production and thermodynamic power of the squeezed thermal reservoir, Phys. Rev. E **93**, 052120 (2016).

[16] J. Klatzow, J. N. Becker, P. M. Ledingham, C. Weinzetl, K. T. Kaczmarek, D. J. Saunders, J. Nunn, I. A. Walmsley, R. Uzdin, and E. Poem, Experimental Demonstration of Quantum Effects in the Operation of Microscopic Heat Engines, Phys. Rev. Lett. **122**, 110601 (2019).

[17] F. L. S. Rodrigues, G. De Chiara, M. Paternostro, and G. T. Landi, Thermodynamics of Weakly Coherent Collisional Models, Phys. Rev. Lett. **123**, 140601 (2019).

[18] K. Hammam, Y. Hassouni, R. Fazio, and G. Manzano, Optimizing autonomous thermal machines powered by energetic coherence, New J. Phys. **23**, 043024 (2021).

[19] M. O. Scully, M. S. Zubairy, G. S. Agarwal, and H. Walther, Extracting work from a single heat bath via vanishing quantum coherence, Science **299**, 862 (2003).

[20] X. L. Huang, T. Wang, and X. X. Yi, Effects of reservoir squeezing on quantum systems and work extraction, Phys. Rev. E **86**, 051105 (2012).

[21] J. Roßnagel, O. Abah, F. Schmidt-Kaler, K. Singer, and E. Lutz, Nanoscale Heat Engine Beyond the Carnot Limit, Phys. Rev. Lett. **112**, 030602 (2014).

[22] L. A. Correa, J. P. Palao, D. Alonso, and G. Adesso, Quantum-enhanced absorption refrigerators, Sci. Rep. **4**, 3949 (2014).

[23] T. F. F. Santos, F. Tacchino, D. Gerace, M. Campisi, and M. F. Santos, Maximally efficient quantum thermal machines fueled by nonequilibrium steady states, Phys. Rev. A **103**, 062225 (2021).

[24] K. Hammam, H. Leitch, Y. Hassouni, and G. De Chiara, Exploiting coherence for quantum thermodynamic advantage, New J. Phys. **24**, 113053 (2022).

[25] B. K. Agarwalla and D. Segal, Assessing the validity of the thermodynamic uncertainty relation in quantum systems, Phys. Rev. B **98**, 155438 (2018).

[26] G. Guarnieri, G. T. Landi, S. R. Clark, and J. Goold, Thermodynamics of precision in quantum nonequilibrium steady states, Phys. Rev. Res. **1**, 033021 (2019).

[27] J. Liu and D. Segal, Thermodynamic uncertainty relation in quantum thermoelectric junctions, Phys. Rev. E **99**, 062141 (2019).

[28] T. Ehrlich and G. Schaller, Broadband frequency filters with quantum dot chains, Phys. Rev. B **104**, 045424 (2021).

[29] P. Menczel, E. Loisa, K. Brandner, and C. Flindt, Thermodynamic uncertainty relations for coherently driven open quantum systems, J. Phys. A: Math. Theor. **54**, 314002 (2021).

[30] A. A. S. Kalaee, A. Wacker, and P. P. Potts, Violating the thermodynamic uncertainty relation in the three-level maser, Phys. Rev. E **104**, L012103 (2021).

[31] A. Rignon-Bret, G. Guarnieri, J. Goold, and M. T. Mitchison, Thermodynamics of precision in quantum nanomachines, Phys. Rev. E **103**, 012133 (2021).

[32] S. Nimmrichter, J. Dai, A. Roulet, and V. Scarani, Quantum and classical dynamics of a three-mode absorption refrigerator, Quantum **1**, 37 (2017).

[33] J. O. González, J. P. Palao, D. Alonso, and L. A. Correa, Classical emulation of quantum-coherent thermal machines, Phys. Rev. E **99**, 062102 (2019).

[34] E. Bäumer, M. Lostaglio, M. Perarnau-Llobet, and R. Sampaio, Fluctuating work in coherent quantum systems: Proposals and limitations, in *Thermodynamics in the Quantum Regime. Fundamental Theories of Physics*, edited by F. Binder, L. Correa, C. Gogolin, J. Anders, and G. Adesso (Springer, Cham, 2018), Vol. 195, pp. 275–300.

[35] M. Lostaglio, Certifying Quantum Signatures in Thermodynamics and Metrology via Contextuality of Quantum Linear Response, Phys. Rev. Lett. **125**, 230603 (2020).

[36] V. Giovannetti, S. Lloyd, and L. Maccone, Advances in quantum metrology, Nat. Photonics **5**, 222 (2011).

[37] K. Bharti, A. Cervera-Lierta, T. H. Kyaw, T. Haug, S. Alperin-Lea, A. Anand, M. Degroote, H. Heimonen, J. S. Kottmann, T. Menke *et al.*, Noisy intermediate-scale quantum algorithms, Rev. Mod. Phys. **94**, 015004 (2022).

[38] F. Campaioli, F. A. Pollock, and S. Vinjanampathy, Quantum batteries, in *Thermodynamics in the Quantum Regime. Fundamental Theories of Physics*, edited by F. Binder, L. Correa,

C. Gogolin, J. Anders, and G. Adesso (Springer, Cham, 2018), Vol. 195, pp. 207–225.

[39] S. Bhattacharjee and A. Dutta, Quantum thermal machines and batteries, Eur. Phys. J. B 2021 9412 **94**, 239 (2021).

[40] R. Alicki and M. Fannes, Entanglement boost for extractable work from ensembles of quantum batteries, Phys. Rev. E **87**, 042123 (2013).

[41] K. V. Hovhannisyan, M. Perarnau-Llobet, M. Huber, and A. Acín, Entanglement Generation is Not Necessary for Optimal Work Extraction, Phys. Rev. Lett. **111**, 240401 (2013).

[42] F. C. Binder, S. Vinjanampathy, K. Modi, and J. Goold, Quantacell: Powerful charging of quantum batteries, New J. Phys. **17**, 075015 (2015).

[43] F. Campaioli, F. A. Pollock, F. C. Binder, L. Céleri, J. Goold, S. Vinjanampathy, and K. Modi, Enhancing the Charging Power of Quantum Batteries, Phys. Rev. Lett. **118**, 150601 (2017).

[44] S. Julià-Farré, T. Salamon, A. Riera, M. N. Bera, and M. Lewenstein, Bounds on the capacity and power of quantum batteries, Phys. Rev. Res. **2**, 023113 (2020).

[45] J.-Y. Gyhm, D. Šafránek, and D. Rosa, Quantum Charging Advantage Cannot Be Extensive without Global Operations, Phys. Rev. Lett. **128**, 140501 (2022).

[46] F. Barra, Dissipative Charging of a Quantum Battery, Phys. Rev. Lett. **122**, 210601 (2019).

[47] D. Farina, G. M. Andolina, A. Mari, M. Polini, and V. Giovannetti, Charger-mediated energy transfer for quantum batteries: An open-system approach, Phys. Rev. B **99**, 035421 (2019).

[48] F. H. Kamin, F. T. Tabesh, S. Salimi, F. Kheirandish, and A. C. Santos, Non-Markovian effects on charging and self-discharging process of quantum batteries, New J. Phys. **22**, 083007 (2020).

[49] K. V. Hovhannisyan, F. Barra, and A. Imparato, Charging assisted by thermalization, Phys. Rev. Res. **2**, 033413 (2020).

[50] F. T. Tabesh, F. H. Kamin, and S. Salimi, Environment-mediated charging process of quantum batteries, Phys. Rev. A **102**, 052223 (2020).

[51] S. Ghosh, T. Chanda, S. Mal, and A. Sen(De), Fast charging of a quantum battery assisted by noise, Phys. Rev. A **104**, 032207 (2021).

[52] S. Zakavati, F. T. Tabesh, and S. Salimi, Bounds on charging power of open quantum batteries, Phys. Rev. E **104**, 054117 (2021).

[53] T. P. Le, J. Levinsen, K. Modi, M. M. Parish, and F. A. Pollock, Spin-chain model of a many-body quantum battery, Phys. Rev. A **97**, 022106 (2018).

[54] D. Rossini, G. M. Andolina, and M. Polini, Many-body localized quantum batteries, Phys. Rev. B **100**, 115142 (2019).

[55] D. Rossini, G. M. Andolina, D. Rosa, M. Carrega, and M. Polini, Quantum Advantage in the Charging Process of Sachdev-Ye-Kitaev Batteries, Phys. Rev. Lett. **125**, 236402 (2020).

[56] D. Rosa, D. Rossini, G. M. Andolina, M. Polini, and M. Carrega, Ultra-stable charging of fast-scrambling SYK quantum batteries, J. High Energy Phys. 11 (2020) 067.

[57] S. Ghosh, T. Chanda, and A. Sen(De), Enhancement in the performance of a quantum battery by ordered and disordered interactions, Phys. Rev. A **101**, 032115 (2020).

[58] L. Peng, W.-B. He, S. Chesi, H.-Q. Lin, and X.-W. Guan, Lower and upper bounds of quantum battery power in multiple central spin systems, Phys. Rev. A **103**, 052220 (2021).

[59] F. Zhao, F.-Q. Dou, and Q. Zhao, Quantum battery of interacting spins with environmental noise, Phys. Rev. A **103**, 033715 (2021).

[60] W. Lu, J. Chen, L.-M. Kuang, and X. Wang, Optimal state for a Tavis-Cummings quantum battery via the Bethe ansatz method, Phys. Rev. A **104**, 043706 (2021).

[61] F. Barra, K. V. Hovhannisyan, and A. Imparato, Quantum batteries at the verge of a phase transition, New J. Phys. **24**, 015003 (2022).

[62] R. Salvia and V. Giovannetti, Extracting work from correlated many-body quantum systems, Phys. Rev. A **105**, 012414 (2022).

[63] S. Ghosh and A. Sen(De), Dimensional enhancements in a quantum battery with imperfections, Phys. Rev. A **105**, 022628 (2022).

[64] N. Friis and M. Huber, Precision and work fluctuations in gaussian battery charging, Quantum **2**, 61 (2018).

[65] E. McKay, N. A. Rodríguez-Briones, and E. Martín-Martínez, Fluctuations of work cost in optimal generation of correlations, Phys. Rev. E **98**, 032132 (2018).

[66] M. Perarnau-Llobet and R. Uzdin, Collective operations can extremely reduce work fluctuations, New J. Phys. **21**, 083023 (2019).

[67] L. P. García-Pintos, A. Hamma, and A. del Campo, Fluctuations in Extractable Work Bound the Charging Power of Quantum Batteries, Phys. Rev. Lett. **125**, 040601 (2020).

[68] A. Crescente, M. Carrega, M. Sassetti, and D. Ferraro, Charging and energy fluctuations of a driven quantum battery, New J. Phys. **22**, 063057 (2020).

[69] F. Caravelli, G. Coulter-De Wit, L. P. García-Pintos, and A. Hamma, Random quantum batteries, Phys. Rev. Res. **2**, 023095 (2020).

[70] R. Salvia and V. Giovannetti, On the distribution of the mean energy in the unitary orbit of quantum states, Quantum **5**, 514 (2021).

[71] F. Barra, Efficiency fluctuations in a quantum battery charged by a repeated interaction process, Entropy **24**, 820 (2022).

[72] B. Çakmak, A. Manatuly, and O. E. Müstecaplıoğlu, Thermal production, protection, and heat exchange of quantum coherences, Phys. Rev. A **96**, 032117 (2017).

[73] J. Monsel, M. Fellous-Asiani, B. Huard, and A. Auffèves, The Energetic Cost of Work Extraction, Phys. Rev. Lett. **124**, 130601 (2020).

[74] G. Francica, F. Binder, G. Guarnieri, M. Mitchison, J. Goold, and F. Plastina, Quantum Coherence and Ergotropy, Phys. Rev. Lett. **125**, 180603 (2020).

[75] F. H. Kamin, F. T. Tabesh, S. Salimi, and A. C. Santos, Entanglement, coherence, and charging process of quantum batteries, Phys. Rev. E **102**, 052109 (2020).

[76] F. Caravelli, B. Yan, L. P. García-Pintos, and A. Hamma, Energy storage and coherence in closed and open quantum batteries, Quantum **5**, 505 (2021).

[77] D. Ferraro, M. Campisi, G. M. Andolina, V. Pellegrini, and M. Polini, High-Power Collective Charging of a Solid-State Quantum Battery, Phys. Rev. Lett. **120**, 117702 (2018).

[78] G. M. Andolina, M. Keck, A. Mari, M. Campisi, V. Giovannetti, and M. Polini, Extractable Work, the Role of

Correlations, and Asymptotic Freedom in Quantum Batteries, Phys. Rev. Lett. **122**, 047702 (2019).

[79] G. M. Andolina, M. Keck, A. Mari, V. Giovannetti, and M. Polini, Quantum versus classical many-body batteries, Phys. Rev. B **99**, 205437 (2019).

[80] S. Gherardini, F. Campaioli, F. Caruso, and F. C. Binder, Stabilizing open quantum batteries by sequential measurements, Phys. Rev. Res. **2**, 013095 (2020).

[81] A. C. Santos, A. Saguia, and M. S. Sarandy, Stable and charge-switchable quantum batteries, Phys. Rev. E **101**, 062114 (2020).

[82] J. Q. Quach and W. J. Munro, Using Dark States to Charge and Stabilize Open Quantum Batteries, Phys. Rev. Appl. **14**, 024092 (2020).

[83] G. T. Landi, Battery charging in collision models with bayesian risk strategies, Entropy **23**, 1627 (2021).

[84] A. C. Santos, B. Çakmak, S. Campbell, and N. T. Zinner, Stable adiabatic quantum batteries, Phys. Rev. E **100**, 032107 (2019).

[85] M. T. Mitchison, J. Goold, and J. Prior, Charging a quantum battery with linear feedback control, Quantum **5**, 500 (2021).

[86] M. Łobejko, P. Mazurek, and M. Horodecki, Thermodynamics of minimal coupling quantum heat engines, Quantum **4**, 375 (2020).

[87] S. Seah, M. Perarnau-Llobet, G. Haack, N. Brunner, and S. Nimmrichter, Quantum Speed-Up in Collisional Battery Charging, Phys. Rev. Lett. **127**, 100601 (2021).

[88] P. Lipka-Bartosik, P. Mazurek, and M. Horodecki, Second law of thermodynamics for batteries with vacuum state, Quantum **5**, 408 (2021).

[89] M. Łobejko, The tight second law inequality for coherent quantum systems and finite-size heat baths, Nat. Commun. **12**, 918 (2021).

[90] R. R. Rodriguez, B. Ahmadi, G. Suarez, P. Mazurek, S. Barzanjeh, and P. Horodecki, Optimal quantum control of charging quantum batteries, arXiv:2207.00094 (2022).

[91] A. Levy, L. Diósi, and R. Kosloff, Quantum flywheel, Phys. Rev. A **93**, 052119 (2016).

[92] S. Seah, S. Nimmrichter, and V. Scarani, Work production of quantum rotor engines, New J. Phys. **20**, 043045 (2018).

[93] G. M. Andolina, D. Farina, A. Mari, V. Pellegrini, V. Giovannetti, and M. Polini, Charger-mediated energy transfer in exactly solvable models for quantum batteries, Phys. Rev. B **98**, 205423 (2018).

[94] S. Tirone, R. Salvia, and V. Giovannetti, Quantum Energy Lines and the Optimal Output Ergotropy Problem, Phys. Rev. Lett. **127**, 210601 (2021).

[95] L. Fusco, M. Paternostro, and G. D. Chiara, Work extraction and energy storage in the Dicke model, Phys. Rev. E **94**, 052122 (2016).

[96] F. Pirmoradian and K. Mølmer, Aging of a quantum battery, Phys. Rev. A **100**, 043833 (2019).

[97] F.-Q. Dou, Y.-Q. Lu, Y.-J. Wang, and J.-A. Sun, Extended Dicke quantum battery with interatomic interactions and driving field, Phys. Rev. B **105**, 115405 (2022).

[98] M. Maffei, P. A. Camati, and A. Auffèves, Probing nonclassical light fields with energetic witnesses in waveguide quantum electrodynamics, Phys. Rev. Res. **3**, L032073 (2021).

[99] C.-K. Hu, J. Qiu, P. J. P. Souza, J. Yuan, Y. Zhou, L. Zhang, J. Chu, X. Pan, L. Hu, J. Li *et al.*, Optimal charging of a superconducting quantum battery, Quantum Sci. Technol. **7**, 045018 (2022).

[100] J. Q. Quach, K. E. McGhee, L. Ganzer, D. M. Rouse, B. W. Lovett, E. M. Gauger, J. Keeling, G. Cerullo, D. G. Lidzey, and T. Virgili, Superabsorption in an organic microcavity: Toward a quantum battery, Sci. Adv. **8**, eabk3160 (2022).

[101] C. Sayrin, I. Dotsenko, X. Zhou, B. Peaudecerf, T. Rybarczyk, S. Gleyzes, P. Rouchon, M. Mirrahimi, H. Amini, M. Brune *et al.*, Real-time quantum feedback prepares and stabilizes photon number states, Nature (London) **477**, 73 (2011).

[102] X. Linpeng, L. Bresque, M. Maffei, A. N. Jordan, A. Auffèves, and K. W. Murch, Energetic Cost of Measurements Using Quantum, Coherent, and Thermal Light, Phys. Rev. Lett. **128**, 220506 (2022).

[103] D. Zhang, X.-M. Wang, T.-F. Li, X.-Q. Luo, W. Wu, F. Nori, and J. You, Cavity quantum electrodynamics with ferromagnetic magnons in a small yttrium-iron-garnet sphere, npj Quantum Inf. **1**, 15014 (2015).

[104] S. P. Wolski, D. Lachance-Quirion, Y. Tabuchi, S. Kono, A. Noguchi, K. Usami, and Y. Nakamura, Dissipation-Based Quantum Sensing of Magnons with a Superconducting Qubit, Phys. Rev. Lett. **125**, 117701 (2020).

[105] M. Um, J. Zhang, D. Lv, Y. Lu, S. An, J.-N. Zhang, H. Nha, M. S. Kim, and K. Kim, Phonon arithmetic in a trapped ion system, Nat. Commun. **7**, 11410 (2016).

[106] L. H. Zaw, Z. Lasmar, C.-H. Nguyen, K.-W. Tseng, D. Matsukevich, D. Kaszlikowski, and V. Scarani, Sculpting bosonic states with arithmetic subtractions, New J. Phys. **24**, 083023 (2022).

[107] A. E. Allahverdyan, R. Balian, and T. M. Nieuwenhuizen, Maximal work extraction from finite quantum systems, Europhys. Lett. **67**, 565 (2004).

[108] J. L. W. V. Jensen, Sur les fonctions convexes et les inégalités entre les valeurs moyennes, Acta Mathematica **30**, 175 (1906).

[109] J. S. Ivan, K. K. Sabapathy, and R. Simon, Operator-sum representation for bosonic Gaussian channels, Phys. Rev. A **84**, 042311 (2011).

[110] C. Guerlin, J. Bernu, S. Deléglise, C. Sayrin, S. Gleyzes, S. Kuhr, M. Brune, J.-M. Raimond, and S. Haroche, Progressive field-state collapse and quantum non-demolition photon counting, Nature (London) **448**, 889 (2007).

[111] As a simple example, consider an atom trajectory $\mathbf{r}(t) = (vt, b, 0)$ crossing a fundamental Gaussian standing-wave cavity mode with mode function $f(\mathbf{r}) = \exp[-(x^2 + y^2)/2w^2]\cos kz$. Then $\Omega(t) = \Omega_0 \exp(-b^2/w^2 - v^2t^2/w^2)$, and $\theta = \Omega_0 \exp(-b^2/w^2)\sqrt{\pi}w/v$, where Ω_0 is the Rabi frequency in the center of the mode.

[112] V. Shaghaghi, V. Singh, G. Benenti, and D. Rosa, Micromasers as quantum batteries, Quantum Sci. Technol. **7**, 04LT01 (2022).

[113] F. G. S. L. Brandão, M. Horodecki, J. Oppenheim, J. M. Renes, and R. W. Spekkens, Resource Theory of Quantum States Out of Thermal Equilibrium, Phys. Rev. Lett. **111**, 250404 (2013).

[114] F. Brandão, M. Horodecki, N. Ng, J. Oppenheim, and S. Wehner, The second laws of quantum thermodynamics, Proc. Natl. Acad. Sci. USA **112**, 3275 (2015).